Astron. Astrophys. 271, 18–24 (1993)

ASTRONOMY AND ASTROPHYSICS

Variability of the Seyfert galaxy Mkn 766 in the ROSAT all sky survey

Silvano Molendi[1], **Tommaso Maccacaro**[2], **and Stefan Schaeidt**[1]

[1] Max-Planck-Institut für extraterrestrische Physik, W-8046 Garching, Germany
[2] Osservatorio Astronomico di Brera, Via Brera 28, I-20121 Milano, Italy

Received August 8, accepted November 8, 1992

Abstract. Results are presented from the Rosat All Sky Survey (RASS) observation of the Seyfert galaxy Mkn 766. Using a technique specifically developed for the analysis of point sources in the RASS we show that Mkn 766 is highly variable. Comparison of the soft X-ray spectrum (0.1-2 keV) with EXOSAT Medium Energy archive data (2-10 keV) clearly shows that the spectrum of Mkn 766 is characterized by a strong soft-excess. The low energy resolution of the PSPC instrument on board the ROSAT spacecraft does not allow to distinguish between different spectral models for the soft-excess. Both a power-law or a thermal component (blackbody or bremsstrahlung) yield an acceptable fit. Of the two thermal models only the first can be accepted since the best-fitting parameters derived for latter are not consistent with bremsstrahlung emission.

A comparison with theoretical models for the soft-excess is presented. The lack of a strong UV bump rules out models in which soft X-ray are produced by Comptonizing UV photons. The soft-excess in the spectrum of Mkn 766 can be fitted with the emission spectrum from an accretion disk. The accretion disk parameters derived from the fit, the mass and the accretion rate, are consistent with those found by comparing the two variability timescales observed in the lightcurve to two fundamental timescales operating in the disk.

Key words: galaxies: individual: Mkn 766 – galaxies: Seyfert – X-rays: galaxies – radiation mechanisms: miscellaneous – accretion, accretion disks

1. Introduction

Since the paper by Arnaud et al. (1985) on Mkn 841 considerable efforts have been devoted to the study of the soft-excess in the X-ray spectrum of AGNs. Although recent observations have shown that, at least for some objects (e.g. NGC1068, Wilson et al. 1992), soft X-rays originate from an extended region around the nucleus, the rapid variability observed in the spectrum of many active galaxies (e.g. NGC5548, Kaastra & Barr 1989), clearly indicates that soft X-rays are also produced in the innermost regions of the nucleus. Thus the study of AGNs at these frequencies can give valuable information on the mechanism powering the nucleus.

In this paper we present the analysis of the Rosat All Sky Survey (RASS) data for Mkn 766. This is a Seyfert 1 Galaxy included in the Extended Medium Sensitivity Survey (EMSS, cf. Gioia et al. 1990) and is part of a comparison study involving all EMSS sources in the RASS (for a preliminary report see Molendi et al. 1992). Observations were performed on the 4^{th} and 5^{th} of December 1990 with the PSPC detector (cf. Pfeffermann et al. 1986) aboard the ROSAT spacecraft. This instrument allows the study of X-ray emission in the 0.1 to 2.4 keV band and has the considerable advantage, over previous X-ray detectors, of having a very low instrumental background. The moderate spectral resolution, $\Delta E/E \simeq 0.4$ at 1 keV, of the PSPC does not allow a very effective discrimination between the different emission models, but the combination of ROSAT data with archive data in other spectral bands can help discriminate amongst different theoretical models.

The outline of the paper is as follows. In Sect. 2 we present the technique used to produce lightcurves of point sources in the RASS and apply it to a sample of 6 constant sources. This technique is described in detail since this is the first time it is presented in a journal. In Sect. 3 we discuss the lightcurve of Mkn 766. We show that the source is strongly variable and that variability extends to both the soft (0.1-0.4 keV) and hard (0.4-2.4 keV) PSPC bands. In Sect. 4 we report on the results of the spectral analysis of Mkn 766. We show that by comparing the PSPC observation with EXOSAT Medium Energy archive data we have strong evidence for two distinct components. In Sect. 5 we compare our observational results for Mkn 766 with models for soft X-ray emission. We show that the soft-excess in Mkn 766 cannot result from the Comptonization of UV photons. An alternative interpretation based on emission from the innermost

Send offprint requests to: S. Molendi

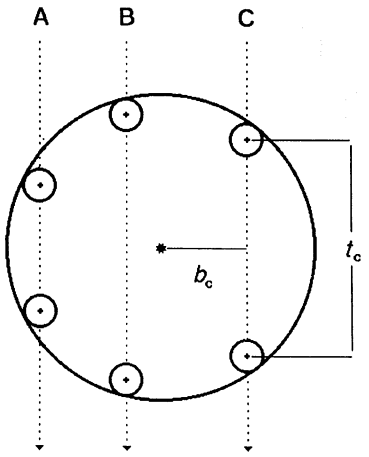

Fig. 1. Schematic representation of three different scans for a source in the Survey. The representation is in detector coordinates. The larger circle represents the detector window, the smaller circles the extraction circles for the source. The length of a scan is a function of the impact parameter b. Only times when the whole extraction circle is inside the detector are accepted

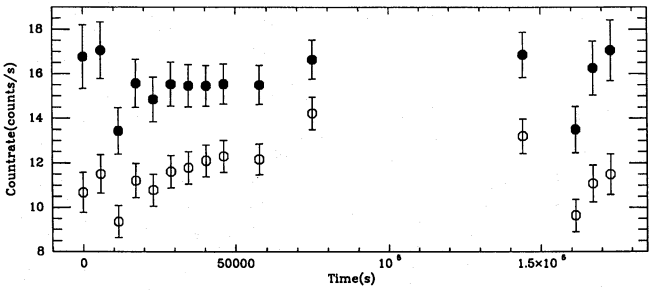

Fig. 2. Raw and corrected lightcurve for the white dwarf WD 0642-166 (Sirius B). The raw lightcurve is represented with empty circles, the corrected one with filled in circles. The time is set to zero on the first scan. A χ^2-test against a constant lightcurve with countrate equal to the average countrate yields a value of χ^2_{red} = 2.79 for the raw lightcurve and χ^2_{red} = 1.05 for the corrected one

regions of an accretion disk is found to be consistent with the data. Finally in Sect. 6 we present a summary of the points discussed in the paper.

2. Lightcurves of point sources in the RASS

During the ROSAT All Sky Survey the satellite scans the sky along great circles perpendicular to the sun position (i.e. each scan passes through the ecliptic poles). During the observation period a source is not continuously in the field of view. In the reference frame of the telescope, a source scans the instrument vertically for a few seconds each orbit. The exact length of a pass depends on the impact parameter b (i.e. the distance between the line described by the source and the center of the detector). The length of the scan increases as b decreases, reaching a maximum of $\simeq$ 30 s in the central scan and decreasing thereafter, cf. Fig. 1.

Raw lightcurves of point sources can be produced by dividing the source counts accumulated in each scan by the duration of the scan.

The first step to estimate the raw countrate of a source is to extract the photons from a circle large enough to contain practically all (i.e. more then 99%) source counts.

By studying the radial profile of a few point-like sources we estimated the radius R_o, containing 99% of the source counts. This radius is a function of the source countrate and of the position within the detector; for sources with raw countrate smaller than $\simeq$ 20 cts/s, averaging over all detector positions, we found $R_o \simeq 400''$. A similar computation performed on the basis of pre-launch simulations (Hasinger 1992, private communication) yields $360''$, the difference being due to the neglection, in the latter, of mirror scattering effects. The alternative approach, which would be to choose a smaller circle and correct for the source counts falling outside is not advisable as the point spread function of the PSPC, at large off-axes angles, is poorly known and cannot be easily corrected for.

The second step in computing the raw lightcurve of a source is the computation of the exposure time for each scan. This is defined as the time during which the whole extraction circle of the source is inside the detector (cf. Fig. 1), and is computed using the attitude information (for a detailed description of this and alternative techniques for computing the exposure time the reader is referred to Belloni 1992). Note that the outermost scans, in which the extraction circle is never completely inside the detector, are ignored. The raw countrate is defined as $rcr = counts/exposure$ and the associated error is $\sigma_{rcr} = \sqrt{counts}/exposure$.

Background subtraction for Survey sources is not performed in the usual way. Selecting a ring around the extracted circle and subtracting photons accumulated in the ring from photons in the circle is not a good way of performing a background subtraction in the Survey. The main reason is that two regions close by, but belonging to different scans, are separated in time by at least 96 minutes (one orbit), and during this time the background may have undergone significant changes (crossing from day to night side or vice versa, solar flares, etc...). Thus this technique is incapable of taking into account temporal variations in the background.

The subtraction technique we apply is the following: we take two circles $900''$ away from the source circle, both centered on the same ecliptic meridian as the source circle and having the same radius. We then average the two raw background lightcurves and subtract the average raw background lightcurve from the raw source+background lightcurve. In this way we are always subtracting data from the same orbit. Note also that we do not need to correct the data for vignetting before the subtraction, since the background and the source+background data are obtained by scanning the detector in the same fashion. We choose two background circles rather than one to take into account possible spatial variations in the cosmic background.

The characteristics of the ROSAT telescope (cf. Trümper 1983) and of the PSPC entrance window (cf. Pfeffermann et al. 1986) introduce systematic variations in the raw countrate.

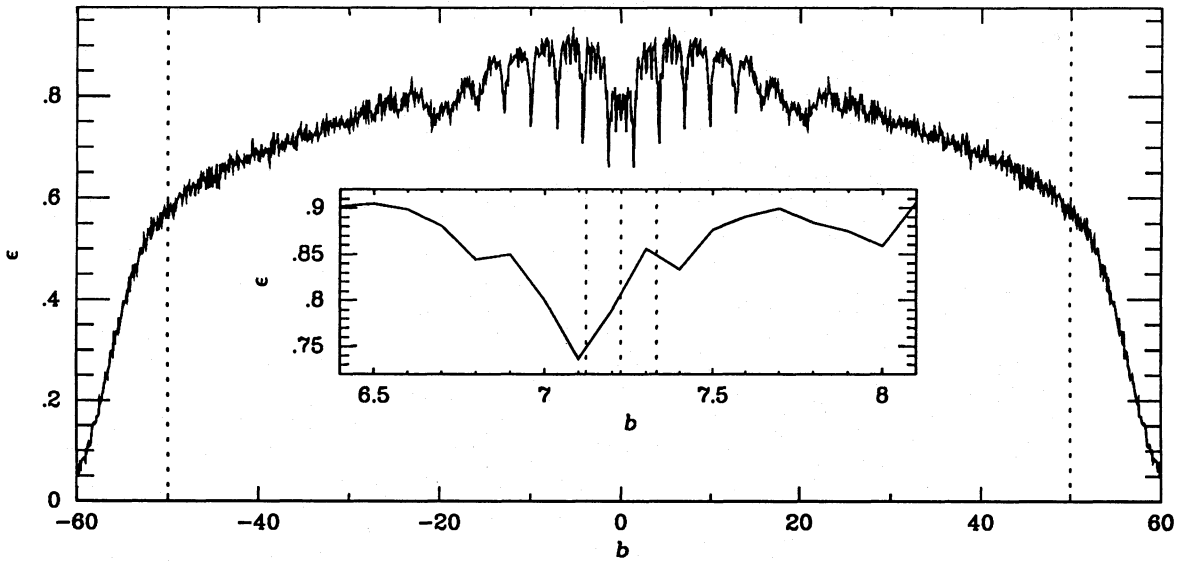

Fig. 3. The ratio of the countrate for a specific scan to the on-axis countrate, ϵ, vs. the impact parameter b of the scan. b is expressed in arcminutes. Only scans falling inside the two vertical dotted lines have been accepted. Inner panel. Blow-up of Fig. 3. The vertical dotted lines indicate $b-\sigma_b$, b and $b+\sigma_b$ for a specific scan. The considerable reduction in ϵ at $b = 7.1$ is related to the presence of a wire

Figure 2 shows the raw lightcurve of the constant white dwarf WD 0642-166.

The correction technique we apply to the raw source lightcurve, (cf. Schaeidt et al. 1992) uses a simulation of a survey observation of a point source. The results of such a simulation are expressed in terms of the efficiency ϵ, i.e. the ratio of the countrate for a specific scan to the on-axis countrate, versus the impact parameter b (cf. Fig. 3). The general increase and decrease of ϵ is due to the vignetting of the telescope, while the strong variations in the central part are the result of shadowing by the support structure and wires of the entrance window (shadowing by the wires occurs only in the central scans where the Point Spread Function, PSF, is sufficiently sharp). The correction performed can be divided into two steps: first the impact parameter b is determined, second the corrected countrate is computed by multiplying the raw countrate by a number derived from the specific value of b determined in step one. The error on the corrected countrate is estimated by propagating the statistical error on the raw source countrate and the error on the impact parameter.

The impact parameter is computed from the attitude data (cf. Belloni 1992). The error on the impact parameter σ_b is given by the deviation of the scan from a straight line. The correction factor cf, which we apply to the raw countrate is given by the expression:

$$cf(b) = \frac{1}{2\sigma_b}\int_{b-\sigma_b}^{b+\sigma_b}\frac{1}{\epsilon(\beta)}d\beta, \qquad (1)$$

and the error on the correction factor is:

$$\sigma_{cf} = \frac{1}{2}\left[\left(cf(b+\sigma_b)-cf(b)\right)^2+\left(cf(b-\sigma_b)-cf(b)\right)^2\right]^{1/2}. \qquad (2)$$

In the inner panel of Fig. 3 we show the case of a specific scan. The central vertical line indicates the impact parameter, on each side we show lines corresponding to $b-\sigma_b$ and $b+\sigma_b$. The corrected countrate is computed by multiplying the raw countrate by the correction factor, while the error on the corrected countrate is obtained by propagating the statistical error on the raw countrate and the error on the correction factor cf. Therefore $\sigma_{ccr} = (\sigma_{cr}^2+\sigma_{cf}^2)^{1/2}$. The lightcurve represented with filled circles in Fig. 2 results from the application of the correction technique to the raw counts shown as open circles in the same figure.

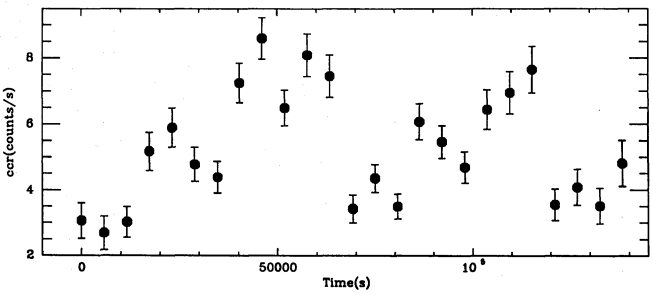

Fig. 4. Corrected lightcurve of Mkn 766

We have tested this technique on a sample of 6 constant sources (white dwarfs). The strong asymmetry of the PSF and the strong gradient in the vignetting function at large off-axes angles are such that corrections applied in the first two and last two scans are highly uncertain. Consequently we have decided to exclude these scans from our analysis (these points are not shown in the figures). In 2 of the 6 objects analyzed we found one scan where the countrate was so low to be consistent with the background countrate. Investigation of the housekeeping data for these two scans showed that both were characterized by unacceptable attitude solution. On the basis of this result we

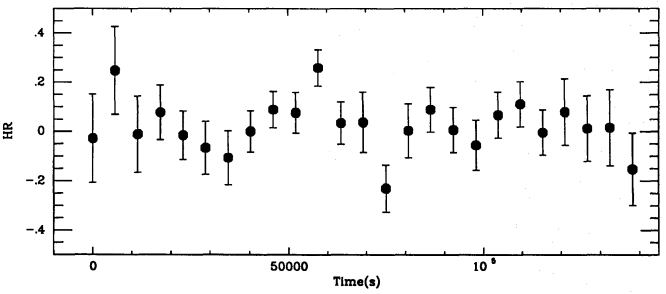

Fig. 5. Hardness ratio lightcurve of Mkn 766. The hardness ratio is defined as $HR = \frac{H-S}{H+S}$, where the S band goes from 0.07 to 0.4 keV and the H band goes from 0.4 to 2.4 keV. The HR curve shows that variability extends to both the soft and hard bands

Table 1. Comparison of the observed lightcurves with constant lightcurves.

Source	$\overline{ccr}$	$\chi^2_{red}/d.o.f.$
WD 0004+330	2.44	1.07/19
WD 0050-332	3.56	1.93/17
WD 0346-011	2.58	1.16/18
WD 0548+000	0.92	0.42/25
WD 1845+019	1.08	1.28/17
WD 0642-166	15.63	1.03/15
Mkn 766	5.31	9.06/25

The constant countrate is set at $\overline{ccr}$, the value of the corrected countrate averaged over all scans.

have decided to include a systematic screening of the housekeeping data in our procedure for all the objects in our sample. No further attitude problems were found. In Table 1 we report the results of a χ^2-test of the observed lightcurves against a constant lightcurve with a countrate equal to the average observed countrate, $\overline{ccr}$, for the sources in our sample. The average value of χ^2_{red} is 1.15, while for one source $\chi^2_{red} \simeq 2$. These results indicate that some residual artificial variability is present in the data. We will assume a source to be variable only if χ^2_{red} exceeds significantly the maximum value found for the white dwarf sample. Reprocessing of the data at a future time may well reduce this somewhat high threshold and allow the investigation of "weaker" variability. At present it seems to us that, due to the large variations in the efficiency curve (cf. Fig. 3), the question of variations of less than $\simeq 40\%$ cannot be addressed with RASS data.

3. The lightcurve of Mkn 766

We have used the technique described in Sect. 2 to compute the lightcurve of Mkn 766 (cf. Fig. 4). This is a type 1 Seyfert Galaxy at a redshift of $z = 0.012$ which has been observed at radio, infrared, optical UV and X-ray frequencies. The electromagnetic spectrum of the source is characterized by a large contribution of the far infrared emission to the bolometric luminosity. Apparent magnitudes, $m_v = 13.57$, $m_b = 14.34$ and $m_u = 14.34$ were obtained from the Veron & Veron Catalog (1991) and an IUE observation was retrieved from the ULDA database. From these data we find no evidence of a blue-UV bump. Mkn 766 was observed in the 0.3-3.5 keV range with the IPC detector onboard the Einstein satellite. About 460 source counts were accumulated during the 2400 s IPC observation, corresponding to a flux of 8×10^{-12} erg/s, in the 0.3-3.5 keV range. The hardness ratio analysis (cf. Maccacaro et al. 1988) yields a photon index of 2.4+/-0.1. Observations in the 2 to 10 keV band have been obtained with the Medium Energy Experiment (ME) onboard the EXOSAT satellite. No observations are available in the Low Energy Experiment (LE) database. The ME spectrum is consistent with a simple power-law model (cf. Table 3), the source is clearly variable in spectral index and flux between different observations. For a more detailed discussion of the ME observations we refer the reader to Sect. 4.

Mkn 766 was observed by ROSAT, in the All Sky Survey, on the 4^{th} and 5^{th} of December 1990. As can be seen from the corrected lightcurve (cf. Fig. 4) the source shows large variations in the countrate. The ratio between the highest and lowest point is about 3 and the χ^2 test yields a value of $\chi^2_{red} \simeq 9$. Variability is not related to a few "events" in the lightcurve, but is a characteristic of the entire lightcurve. In other words eliminating any 2 or 3 data points will not make the variability go away. Furthermore large amplitude variations, more than a factor of 2, are observed between different scans, and the variability pattern of the source is completely different from that of the correction function. Finally a check of the quality of the attitude data revealed no indication of the problems discussed in the previous section.

Having determined that Mkn 766 is variable it is important to establish the nature of this variability. The observed lightcurve is consistent with two main "events", during which the source brightened, by a factor of $\simeq 3$, separated by fast transitions to a low state. The duration of the events is comparable ($\simeq 10 - 12$ hours), while a possible third event is only partially covered in our dataset. The duration of the transition to the low state cannot be determined very precisely from our dataset. Direct inspection of the lightcurve indicates that the first transition maybe somewhat longer then our sampling time (96 minutes), while the second is shorter. Using the technique described in Sect. 2 we produced lightcurves of Mkn 766 in the soft band, S ($E \simeq 0.07$ to $E \simeq 0.4$ keV), and the hard band, H ($E \simeq 0.4$ to $E \simeq 2.4$ keV), from these we computed the hardness ratio lightcurve ($HR = \frac{H-S}{H+S}$). Inspection of the HR curve (cf. Fig. 5) shows that variability extends both to the soft and hard bands.

4. The spectrum of Mkn 766

Spectral analysis was performed using version 7.1 of the XSPEC model-fitting program. The PSPC spectrum of Mkn 766 is consistent with a simple power-law model, with a photon index $\Gamma = 2.7$ and a normalization of 1.4×10^{-2} photons $s^{-1}cm^{-2}keV^{-1}$ at 1 keV, plus an absorbing column of $3.3 \times 10^{20} cm^{-2}$, corresponding to a 0.1 to 2.4 keV unabsorbed flux of 1.5×10^{-10} ergs s^{-1} cm^{-2}. The absorption column measured in the radio band,

Table 2. Comparison of the best fit for the full PSPC dataset, with the best fit for the very high (VHS) and very low state (VLS).

Data set	I^a	Γ	N_H^b	$\chi^2_{red}/d.o.f.$
Total	1.42	$2.73^{3.00}_{2.48}$	$3.28^{3.98}_{2.64}$	0.89/18
VHS	0.83	$2.71^{2.89}_{2.53}$	3.28	1.14/08
VLS	1.84	$2.70^{2.86}_{2.53}$	3.28	0.86/09

The assumed model is a power-law with absorption. Confidence intervals are 90% confidence intervals.
[a] Normalization in units of 10^{-2} photons cm^{-2} s^{-1} keV^{-1} at 1 keV.
[b] Hydrogen column density in units of 10^{20}cm^{-2}.

1.72×10^{20} cm^{-2} (Dickey et al. 1990), is significantly smaller than the one determined from the X-ray data (cf. Table 2).

The hardness ratio lightcurve in Fig. 5 indicates that the spectrum of Mkn 766 remained essentially constant at a time when the countrate of the source varied considerably. We have quantified this qualitative result by performing spectral analysis of the source in different states. We analyzed pulse height spectra for the very-high state (2 scans with the highest countrates) and very-low state (6 scans with the lowest countrates). We fitted the high and the low state with a single power-law model, keeping the absorption column fixed at the value found for the full dataset. As shown in Table 2, the photon index is constrained between 2.5 and 3.0 for all three datasets.

Fits with a thermal component, blackbody or bremsstrahlung, plus absorption are significantly worse than the power-law one. In both cases the fits fail to account for the high energy part of the spectrum.

To better understand the X-ray energy distribution of Mkn 766 we decided to analyze 5 EXOSAT Medium Energy (ME) spectra, which we retrieved from the EXOSAT archive. All ME spectra are consistent with a single power-law model (cf. Table 3), absorption plays a negligible role and has been fixed to the galactic value. The spectral index varies between different observations. The average value 1.95 is significantly smaller than the one found in the 0.1 to 2.4 keV band. We consider this as evidence for two independent components respectively dominating the soft and the hard X-ray bands. We note that the presence of a steep component dominating at low energies, $E < 1$ keV, the so called "soft-excess", is a common feature in Seyfert galaxies (e.g. Turner & Pounds 1989).

To better determine the properties of the soft-excess we compared the PSPC data with two component models, the first modeling the high energy part of the spectrum, the second the soft-excess. We chose a power-law of photon index $\Gamma = 1.7$, the average value found for Seyferts in the 2-10 keV band (cf. Turner & Pounds 1989), as the first component, and tested three different models: power-law, thermal bremsstrahlung and blackbody, for the second. All three models yield acceptable fits to the data (cf. Table 4)

Note that the N_H derived from the blackbody+power-law fits, unlike the ones derived from the bremsstrahlung+power-law and the power-law+power-law fits is consistent with the N_H extrapolated from the radio maps.

Table 3. Best fits with a single power-law model to the different ME observations.

Obs.	Date[c]	I^a	Γ	$\chi^2_{red}/d.o.f.$
1	85.363	0.86	$1.77^{1.92}_{1.62}$	1.65/15
2	85.364	1.05	$2.07^{2.25}_{1.89}$	1.31/15
3	85.364	1.17	$2.16^{2.31}_{2.02}$	0.91/13
4	85.365	1.09	$1.98^{2.11}_{1.86}$	1.31/16
5	86.001	0.69	$1.52^{1.98}_{1.05}$	1.20/05

The hydrogen column density, N_H, is fixed to the galactic value of 1.72×10^{20} cm^{-2}. Confidence intervals for the photon indices are 90% confidence intervals.
[a] Normalization in units of 10^{-2} photons cm^{-2} s^{-1} keV^{-1} at 1 keV.
[c] Date of the ME observation.

Table 4. Best fits to the PSPC data for 2 component models.

Model	I_1^a	I_2^a	C_2^d	N_H^b	$\chi^2_{red}/d.o.f.$
PL+PL	0.65	0.76	$3.47^{4.59}_{2.56}$	$4.19^{6.17}_{2.82}$	0.81/17
PL+BR	1.01	0.30	$0.23^{0.35}_{0.16}$	$3.21^{4.34}_{2.32}$	0.67/17
PL+BB	1.09	0.13	$0.10^{0.11}_{0.08}$	$2.15^{3.09}_{1.53}$	0.65/17

The high energy component is a power-law with photon index fixed at 1.7. I_1 and I_2 are respectively the normalization of the first and second component. Confidence intervals are 90% confidence intervals for the 2 interesting parameters.
[a] Normalization in units of 10^{-2} photons cm^{-2} s^{-1} keV^{-1} at 1 keV.
[b] Hydrogen column density in units of 10^{20}cm^{-2}.
[d] The values reported in this column are respectively the photon index for the power-law+power-law model (PL+PL) and the temperature in keV for the power-law+bremsstrahlung (PL+BR) and the power-law+blackbody (PL+BB) models.

Urry et al. (1989) fitted the IPC+MPC data of Mkn 766 with a two component model, a blackbody with $kT = 18.6$ eV plus a power-law with photon index $\Gamma = 1.76$ and absorption. We found that the PSPC data are not consistent with this model. No acceptable fit can be obtained as long as the blackbody contributes significantly to the low energy flux and has a temperature of < 60 eV (see Table 4).

From the blackbody normalization (Table 4) a size of $R \simeq 3\times10^{11}$ cm is derived for the emitting region. From the bremsstrahlung normalization, by limiting the size of the emission region to be $R \leq c\Delta t_{short}$ (Δt_{short} is the short variability timescale, which we take to be of the order of the orbit time) we find a minimum density of $n \simeq 1.2\times10^{12}$cm^{-3}. The optical depth for electron scattering is then $\tau_{es} \simeq 138$, while the effective optical depth is $\tau^* \equiv (\tau_{abs} * \tau_{es})^{1/2} \simeq 6.3\times10^{-3}$, where τ_{abs} is the optical depth for absorption. Thus, though photons emitted may freely escape without being absorbed, they undergo a large number of scatterings, significantly distorting the original bremsstrahlung spectrum (the Compton parameter defined as $y \equiv \frac{4kT}{m_e c^2}\tau_{es}^2$ is 8.2). We conclude that the parameters required to model the soft-excess in terms of thermal bremsstrahlung emission are inconsistent.

Fluxes and luminosities for the different model are reported in Table 5.

Given the fast variability and the large luminosity variations we have checked whether our source satisfied the $\Delta L/\Delta t$ criterium, $\Delta L \leq \eta \frac{m_p c^4}{\sigma_t} \Delta t$ (cf. Fabian 1979), where η is the efficiency with which matter is transformed into radiation, we take $\eta = 1/10$, σ_T is the Thompson cross section and m_p is the proton mass. By substituting the short timescale, which we assume to be of the order of the orbit time, $\Delta t \simeq 96$ minutes, we find that $\Delta L \leq 1.2 \times 10^{45}$erg s^{-1}. This is consistent with the observed value of the luminosity variation $\Delta L_{obs} \simeq 10^{44}$erg s^{-1}.

5. Comparison with theoretical models

If soft X-rays are produced by Compton scattering of UV photons on energetic electrons, as in the soft-excess models discussed by Zdziarski & Coppi (1991), we expect a strong correlation between flux and spectral index. Since in Mkn 766 we see no significant spectral change related to the strong variability we conclude that this model does not apply to our source. Note also that in the Comptonization model the strength of the soft-excess is related to the strength of the UV bump and that in Mkn 766 we have no evidence of a UV bump (cf. Fig. 6).

An alternative interpretation is that the soft X-ray emission originates from a "hot" accretion disk. This is in agreement with the lack of a strong UV bump and the high X-ray to UV flux ratio (cf. Fig. 6), the hot disk radiates mainly in the XUV and soft X-rays rather than in the UV. Another point in favor of the accretion disk model is that the low energy part of the X-ray spectrum can be fitted with a thermal component.

Table 5. Fluxes and luminosities for the various models.

Model	Flux	Energy Range	Luminosity
PSPC Pow.law	1.51	0.1-2.4 keV	9.7
ME Pow.law[e]	0.32	2-10 keV	2.0
Bremsstrahlung	1.31	0.1-2.4 keV	8.3
Blackbody	0.87	0.1-2.4 keV	5.6

Fluxes are in units of 10^{-10} erg cm^{-2} s^{-1}. Luminosities are in units of 10^{43} erg s^{-1}. Values in the 3^{rd} and 4^{th} row are derived from the thermal component plus power-law fits to the PSPC data. Luminosities are computed assuming $H_o = 50$ km s^{-1} Mpc^{-1}.
[e] The numbers reported here refer to the 1^{st} ME observation (observation date 85.363).

We further tested this model by fitting the emission spectrum of an accretion disk to the PSPC data. We chose to use a disk radiating locally like a modified blackbody, in agreement with the physical conditions expected in a "hot" disk (cf. Shakura & Sunyaev 1973). We also included a power-law component with fixed slope $\Gamma = 1.7$ to reproduce the high energy part of the spectrum and absorbed both components with a fixed equivalent hydrogen column density of $N_H = 2.0 \times 10^{20}$ cm^{-2}. The fit was performed using the disk model "disko" available

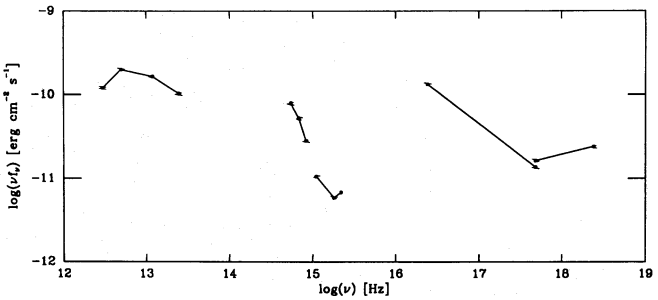

Fig. 6. Infrared to X-ray spectrum of Mkn 766. Points joint by a line indicate simultaneous observations. Infrared data have been extracted from the IRAS database, optical data are taken from the Veron & Veron catalogue (1991). UV data have been extracted from the IUE database. Soft X-ray data are from our Survey observation and hard X-ray data from the EXOSAT ME database. In the X-rays we show the best fitting power-law for the PSPC data and for the ME data collected on day 363 of 1985

in the XSPEC program. The viscosity parameter α was fixed at the value of 0.1. The free parameters of the model are the inclination of the disk with respect to the line of sight, which we leave free to vary between 0 and 80 degrees, the mass of the black hole, which we express in units of solar masses and the accretion rate $\dot{m}$, which we express in units of the critical accretion rate $\dot{M}_{cr}$, defined by the relationship $L_{edd} = \eta \dot{M}_{cr} c^2$, where L_{edd} is the Eddington luminosity and η is the efficiency with which matter is converted into radiation ($\eta = 1/12$ for a Newtonian disk). The model yields an acceptable fit to the data, $\chi^2 = 1.1$ for 17 d.o.f., with best fitting values of $\dot{m} = 0.62$ and $m = 2 \times 10^6$. In Fig. 7 we show the 68%, 90% and 99% confidence contours for the two interesting parameters m and $\dot{m}$. Note that the horizontal lines constraining the mass in the range 7×10^5 to 3×10^6 solar masses result from the limits set on the inclination angle (for small value of the mass the disk is seen face on while for high values of the mass it is seen edge on.)

An independent estimate of the mass and accretion rate can be obtained by comparing the two timescales observed in the lightcurve of Mkn 766 to timescales on which we expect variations in the emission spectrum of an accretion disk. We assume that the long rise, $\simeq 11$ hours, is related to a variation of the accretion rate and that the short decrease, $\simeq 96$ min, is connected to a thermal instability in the disk. Consequently we equate the long timescale, 11 hours, to the the radial drift timescale $t_r = \alpha^{-1}(r/h)^2\omega^{-1}$, where α is the viscosity parameter, h is the disk scale height, r is the distance from the central object and ω is the angular velocity, and the short timescale, 96 minutes, to the thermal timescale $t_{th} = 4/3\alpha^{-1}\omega^{-1}$, the value of the viscosity parameter α is fixed at 0.1. We find that for each radius there exists a pair of values of m and $\dot{m}$ satisfying the above constraints, and that for radii between $r_{min} \simeq 1.5 r_{in}$ and $r_{max} \simeq 3.2 r_{in}$, where r_{in} is the innermost radius of the disk, the values are within the 90% confidence region (see Fig. 7). Thus the independent analysis of the spectrum and of the

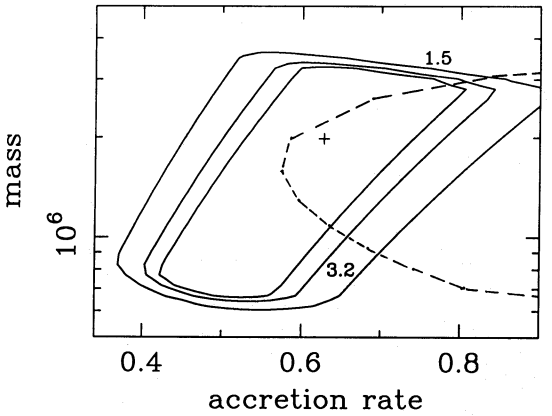

Fig. 7. Confidence contours (68%, 90% and 99%) for the accretion rate $\dot{m}$ and the black hole mass, m. The cross indicates the best fitting value for the parameters. Points on the dashed curve satisfy the condition t_r = 11 hours and t_{th} = 96 minutes. Also indicated are the values of the disk radius at which the dashed line crosses the 90% confidence region

lightcurve of Mkn 766, in the context of accretion disk models, leads to consistent values of the mass and accretion rate.

An independent estimate of the mass for Mkn 766, based on the analysis of the broad Hβ line, cf. Padovani et al. 1990, yields a somewhat higher value of 6.8 $\times 10^6$ M$_\odot$.

6. Conclusions

Using a technique specifically developed for the analysis of point sources in the RASS we have shown that Mkn 766 is strongly variable on timescales of a few hours.

There is no significant spectral variation associated to the variation in the lightcurve.

The comparison of the PSPC data with archive EXOSAT ME data clearly shows that there are two components in the spectrum of Mkn 766, the first dominating the soft X-ray band, the second dominating the hard X-ray band.

The soft-excess can be modeled with a power-law or a thermal component. Blackbody and bremsstrahlung give an equally acceptable fit, but the latter must be rejected because the inferred parameters are not consistent with bremsstrahlung emission.

A comparison with theoretical models shows that the soft-excess in Mkn 766 cannot be produced by Comptonization of UV photons, instead it can be interpreted as emission from the inner region of an accretion disk. The accretion disk parameters m and $\dot{m}$ determined from the spectral fitting are consistent with those found by equating the two timescales observed in the lightcurve to two fundamental timescales operating in the disk.

Acknowledgements. The SASS and the EXSAS teams are thanked for technical support in the data acquisition and reduction. Tom Fleming is thanked for supplying the white dwarf sample data. Roland Walter is thanked for help in retrieving the IUE spectrum of Mkn 766 from the ULDA database. Tomaso Belloni, Andrea Comastri, Günther Hasinger, Joachim Trümper and Andrzej Zdziarski are thanked for useful discussions. S.M. acknowledges financial support from MPE. T.M. acknowledges financial support from ASI.

References

Arnaud, K.A., Branduardi-Raymont, G., Culhane, J.L., Fabian, A.C., Hazard, C., McGlynn, T.A., Shafer, R.A., Tennant, A.F. and Ward M.,J., 1985 *MNRAS*, 217, 105

Belloni, T. 1992 *in preparation*

Dickey, J. M., and Lockman, F. J. 1990, *Ann. Rev. Astr. Ap.*, 28, 215

Fabian, A.C. 1979, *Proc.Roy.Soc.*, 336, 449

Gioia I., Maccacaro, T., Schild, R., Wolter, A., Stocke, J., Morris, S., and Henry, J.P. 1990 *ApJS*, 72, 567

Hasinger, G. 1992, *private communication*

Kaastra, J.S., and Barr, P. 1989 *A&A*, 226, 59

Maccacaro, T., Gioia, I.M., Wolter, A., Zamorani, G. and Stocke, J.T. 1988, *ApJ*, 326, 680

Molendi, S., Maccacaro T. and Brinkmann, W. 1992, in: 2^{nd} *Garching Workshop on the X-ray Emission from Active Galactic Nuclei and the Cosmic X-ray Background,* W. Brinkmann and J. Trümper (eds.) *MPE Report* 235, 216

Padovani, P., Burg, R. and Edelson R.A. 1990, *ApJ*, 353, 438

Pfeffermann, E., Briel, U.G., Hippmann, H., Kettenring, G., Metzner, G., Predehl, P., Reger, G., Stephan, K.H., Zombeck, M.V., Chappell, J. & Murray, S.S.: 1986, *SPIE*, 733, 519

Schaeidt, Hasinger and Trümper J. 1992, in: 2^{nd} *Garching Workshop on the X-ray Emission from Active Galactic Nuclei and the Cosmic X-ray Background,* W. Brinkmann and J. Trümper (eds.) *MPE Report* 235, 216

Shakura, N.I. and Sunyaev, R.A. 1973, *A&A*, 24, 337

Trümper, J. 1983, *Adv. Space Res.* 4, 241

Turner, T.J. and Pounds, K.A. 1989, *MNRAS*, 240, 833

Urry, C.M., Arnaud, K., Edelson, R.A., Kruper, J.S., and Mushotzky, R.F. 1989 in: *Proced. 23rd ESLAB Symp. on Two Topics in X-ray Astronomy,* Bologna, 975

Veron-Cetty, M.-P. and Veron, P. *A Catalogue of Quasars and Active Nuclei (5^{th} Edition 1991)* ESO Scientific Report 10

Wilson, A.S., Elvis, M., Lawrence A. and Bland-Hawthorn, J. 1992, *ApJL*, 391, 75

Zdziarski, A.A., Coppi, P.S. 1991, *ApJ*, 376, 480

This article was processed by the author using Springer-Verlag LaTeX A&A style file version 3.